

Influence of Growth Rate on Eutectic Spacing, Microhardness, and Ultimate Tensile Strength in the Directionally Solidified Al-Cu-Ni Eutectic Alloy



ÜMIT BAYRAM and NECMETTİN MARAŞLI

In this work, the mechanical properties of the Al-Cu-Ni eutectic alloy, Al-32.5 wt pct Cu-1 wt pct Ni, were investigated in terms of the dependency on growth rates. The Al-Cu-Ni eutectic alloy was directionally solidified at a constant temperature gradient, $G = 4.93 \text{ K mm}^{-1}$, with a wide range of growth rates ($V = 9.25$ to $2056.68 \mu\text{m s}^{-1}$) using a Bridgman-type directional solidification furnace. The eutectic spacing (λ), microhardness (HV_T), and ultimate tensile strength (σ_{UTS}) were measured with standard techniques. The dependences of λ , HV_T , and σ_{UTS} on V for directionally solidified Al-Cu-Ni eutectic alloy were experimentally obtained using regression analysis. The results obtained in the present work were compared with the similar experimental results in the literature. Finally, the elastic energy dependence on growth rates for Al-32.5 wt pct Cu-1 wt pct Ni alloy was determined from their nominal stress-strain plots.

<https://doi.org/10.1007/s11663-018-1404-7>

© The Minerals, Metals & Materials Society and ASM International 2018

I. INTRODUCTION

SOLIDIFICATION from the melt is an essential step in nearly all established sequences of metal processing. The solidification and melting are phase transformations between solid and liquid phases of the materials. Understanding the mechanism of solidification is crucial in controlling the electrical, thermal, and mechanical properties of metals.^[1]

Directionally solidified binary or ternary eutectics can produce well-aligned regular structures consisting of fibrous (rodlike) or lamellar constituents. Such structures may offer substantial increases in high-temperature strength, fracture properties, or creep resistance over those of conventionally cast alloys.^[2] The directional solidification method was first used in the 1960s to produce a turbine blade.^[3] This method provides understanding of the relationship between alloys and their microstructure, process conditions, and geometry. Additionally, rapid solidification has been applied to aluminum alloys to improve both individual and combinations of properties in conventional alloys and

thermal stability and elastic stiffness by means of nonconventional alloy additions that are detrimental at normal rates of solidification.^[4]

Commercial aluminum and its alloys can be divided into three grades: work-hardenable wrought compositions, including the metal itself in various grades of purity (1xxx series); with or without solid solution alloying additions of Mg (5xxx series); or with dispersion hardening additions of Mn (3xxx series) age-hardenable wrought compositions, embracing those based on Al-Cu, Al-Mg-Si, and Al-Zn-Mg (2xxx, 6xxx, and 7xxx series, respectively).^[4] The 2xxx series (Al-Cu alloys) have been used extensively in the cast and wrought form where strength and toughness are required. These alloys exhibit high strength and hardness at room and elevated temperatures. Also, copper is typically the alloy basis for improved mechanical properties at elevated temperature, often with nickel additions.^[5]

Considering the studies performed,^[6–10] some workers examined the Al-Cu-Ni system due to the interesting feature of thermoelastic martensitic transformation revealed by specific compositions of these alloys. This feature is answerable for the original mechanical treatment of these alloys, such as superplasticity, stress-induced martensitic transformation, and the shape memory effect.^[11] As can be seen from the literature,^[12–36] the experiments on directional solidification were usually performed within a growth range of 2.0 to $500 \mu\text{m s}^{-1}$ at a constant low-temperature gradient by using a Bridgman-type growth apparatus, and the influence of the growth rate on the microstructure parameters and microhardness was determined from the experimental results.

ÜMIT BAYRAM is with the Department of Physics, Faculty of Science, Erciyes University, 38039 Kayseri, Turkey. NECMETTİN MARAŞLI is with the Department of Metallurgical and Materials Engineering, Faculty of Chemistry and Metallurgical Engineering, Yıldız Technical University, 34210 Istanbul, Turkey. Contact email: nmarasli@yildiz.edu.tr

Manuscript submitted April 3, 2018.

Article published online September 17, 2018.

In the directional growth experiments, the experimental work with a high growth rate (HGR, higher than the $500 \mu\text{m s}^{-1}$) is more difficult.

The first aim of the present work was to directionally solidify the Al-Cu-Ni eutectic alloy with HGRs as well as low growth rates (LGRs) at a constant temperature gradient. The second aim of this work was to experimentally investigate the influence of V on the values of λ_T , HV_T , and σ_{UTS} for the directionally solidified Al-Cu-Ni eutectic alloy. Finally, the elastic energy dependence on growth rates for Al-32.5 wt pct Cu-1 wt pct Ni alloy was determined from the nominal stress-strain plots.

II. EXPERIMENTAL PROCEDURE

The experiments were performed in several steps for Al-Cu-Ni eutectic alloy, including the following: preparation of the alloy, microstructural observation and measurement of solidification parameters, eutectic spacing, microhardness, and ultimate tensile strength (UTS). Details for these steps are given in Sections II-A through II-D.

A. Preparation of Alloy and Observation of Microstructure

In the present study, to grow the eutectic α (Al solution) and θ (CuAl_2) phases from ternary liquid, the composition of the alloy was taken as Al-32.5 wt pct Cu-1 wt pct Ni. Molten Al-32.5 wt pct Cu-1 wt pct Ni alloy was prepared from 99.99 pct pure aluminum, 99.99 pct pure copper, and 99.95 pct pure nickel using a vacuum melting furnace. The molten alloy was poured into graphite crucibles (4-mm ID, 6.35-mm OD, and 200-mm length) held in a hot filling furnace at approximately 50 K above the melting point of the eutectic alloy. The molten alloy in the crucible was directionally solidified to obtain a completely full specimen. Each specimen was then placed in a Bridgman-type furnace within a graphite cylinder (300-mm length, 10-mm ID, and 40-mm OD). Directional solidification of the samples was done at a constant temperature gradient of 4.93 K mm^{-1} with different growth rates from 9.25 to $2056.68 \mu\text{m s}^{-1}$ with the help of different synchronous motors.

In practice, there are six kinds of commercial synchronous motors (1, 2, 5, 10, 20, and 60 rps). The maximum growth rate of $500 \mu\text{m s}^{-1}$ can be obtained with a 60 revolutions s^{-1} synchronous motor at a constant temperature gradient. In the present work, a

driving system was constructed by using a hand drill's motor to obtain HGRs (from 212.45 to $2056.68 \mu\text{m s}^{-1}$) at a constant temperature gradient. Applied voltages v_s pulling rates or pulling rates v_s growth rates obtained with the constructed driving system are given in Table I. The details of the experimental procedure and Bridgman-type furnace are given in References 37 through 39.

To reveal the microstructures on samples, some metallographic processes were carried out on the sample. The quenched sample was cut into lengths typically of 15 mm. The transverse and longitudinal sections of the specimens were flattened with several SiC papers, and samples were cold mounted with the help of epoxy resin. After polishing, the samples were etched with a Keller's microetchant (1.5 mL HCl, 1 mL HF, 2.5 mL HNO_3 , and 95 mL H_2O) for 40 to 45 seconds. The microstructures of samples were photographed with a light optical microscope and a LEO scanning electron microscope (SEM). However, the resolution of the optical microscope was too poor to see the microstructure of the samples solidified with HGRs; thus, the microstructures of samples solidified at all growth rates (ALLGRs) were photographed with an SEM. Some typical SEM images from the longitudinal and transverse sections of directionally solidified Al-Cu-Ni eutectic samples are shown in Figure 1.

B. Measurements of Solidification Parameters and Eutectic Spacing

The temperature of water in the reservoir was kept at approximately 10°C to an accuracy of $\pm 0.3 \text{ K}$ using a Poly Science digital 9102 model heating/refrigerating circulating bath, and the temperature in the sample was controlled to an accuracy of $\pm 0.1 \text{ K}$ by using a Eurotherm 905S type controller. The temperature in the specimen was measured with 0.25-mm diameter insulated 4 K type thermocouples fixed within the sample with spacing of 4 to 6 mm. Four thermocouples were positioned with a spacing of 4 to 6 mm and stuck together with silicone elastomer glue. Before inserting the thermocouples into the alumina, the photographs of thermocouple positions were taken to measure the distance between thermocouples (ΔT). All thermocouples were then inserted together into alumina tubes, 1.5-mm OD \times 1.2-mm ID \times 100-mm length, used to insulate the thermocouples from the melt, and the ends of the thermocouples were then connected to the measurement unit, which consisted of a data logger and computer. During the annealing period, the temperatures on the solid and liquid phases were continuously recorded by the stationary thermocouples with a data logger *via* computer during the growth. When the solid/liquid interface was at the second thermocouple, the temperature difference between the first and second thermocouples (ΔT) was read from the data-logger record. The temperature gradient ($G = \Delta T/\Delta X$) for each sample was determined using the measured value of ΔT and the known value of ΔX .

The time taken for the solid-liquid interface passes through the thermocouples separated by known distances was read from the data-logger record. Thus, the value of the growth rate ($V = \Delta X/\Delta t$) for each sample was determined using the measured values of Δt and ΔX .

Table I. Applied Voltage v_s Pulling Rates or Pulling Rates v_s Growth Rates Obtained with Constructed Driving System for Al-32.5 Wt Pct Cu-1 Wt Pct Ni Alloy

Applied Voltage (Direct Current)	Pulling Rate ($\mu\text{m s}^{-1}$)	Growth Rate ($\mu\text{m s}^{-1}$)
1.0	1034.58	496.72
2.1	2112.83	1024.45
2.9	3086.15	1532.54
3.8	4246.26	2056.68

The estimated error in the measurements of the temperature gradient, G , can be determined with a fractional total uncertainty in G , which can be expressed as

$$\left| \frac{\Delta G}{G} \right| = \left| \frac{\Delta T^*}{\Delta t} \right| + \left| \frac{\Delta X^*}{\Delta X} \right|, \quad [1]$$

where ΔT^* is the uncertainty in the temperature measurements, ΔX^* is the uncertainty in the distance measurements, ΔT is the temperature difference between two fixed points, and ΔX is the distance between two fixed thermocouples.

The distances between two thermocouples were measured from the photographs of the thermocouple's positions to an accuracy of $\pm 5 \mu\text{m}$. The fixed distances between two thermocouples are about 4 to 5 mm. The fractional uncertainty in the measurements of the fixed distances is 0.2 pct.

To determine the uncertainty in the temperature measurements, the thermocouples were calibrated by detecting the melting point of the binary alloy. The uncertainty in the temperature measurements (ΔT^*) at the melting temperature of binary alloys was about 1 K. The temperature difference between the two fixed thermocouples ($\Delta T = T_1 - T_2$) reading was about 80 to 100 K. The uncertainty in the temperature measurements is about 1.3 pct. Therefore, the total fractional uncertainty in the measurements of the temperature gradient is approximately 1.5 pct.

The estimated error in the measurements of the growth rate, V , can be expressed as

$$\left| \frac{\Delta V}{V} \right| = \left| \frac{\Delta X^*}{\Delta X} \right| + \left| \frac{\Delta t^*}{\Delta t} \right|, \quad [2]$$

where Δt^* is the uncertainty in the time measurements and Δt is the time taken for the solid-liquid interface passes through two of the thermocouples. The fractional uncertainty in the measurements of the distances was about 0.3 pct. It can also be seen from Table II that the time taken for the solid-liquid interface to pass through two of the thermocouples is about 80 seconds at higher growth rates. Thus, the uncertainty in the time measurements is about 1.3 pct and that in the growth rate measurements is approximately 2 pct.

Two samples were studied under the same solidification conditions for each growth rate: one of them for microstructure and microhardness measurements and the other for UTS measurements.

The values of eutectic spacing were measured from the photographs of microstructures taken from the transverse and longitudinal sections of the samples with a linear intersection method.^[25] In the measurements of microstructure parameters, 30 to 40 values of eutectic spacing for each temperature gradient were measured to increase statistical sensitivity. Therefore, the statistical error in the measurements of the microstructures was minimized and is given in Table II. The λ values obtained from the transverse sections are more reliable than those of longitudinal sections of the samples.^[26, 27]

As shown in Figure 1, Al-32.5 wt pct Cu-1 wt pct Ni has fine cellular eutectic microstructure with increasing growth rates.

C. Measurements of Microhardness with the Vickers Hardness Method

One of the purposes of the present work is to reveal the relationships between the solidification processing parameters with the microhardness for directionally solidified Al-32.5 wt pct Cu-1 wt pct Ni alloy. The Vickers hardness (HV) is the ratio of a load applied to the indenter to the surface area of the indentation. This is given by

$$\text{HV} = \frac{2P \sin \theta/2}{d^2}, \quad [3]$$

where HV is the Vickers microhardness in N mm^{-2} , P is the applied load (N), d is the mean diagonal of the indentation (mm), and θ is the angle between opposite faces of the diagonal indenter (136 deg). Microhardness measurements in the present work were made with a Future-Tech FM-700 model hardness measuring test device using a 10- to 50-g load and a dwell time of 10 seconds, giving a typical indentation depth of about 40 to 60 μm , which is significantly smaller than that of the original solidified samples.

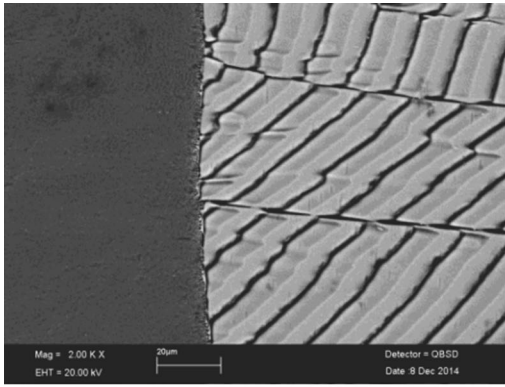
Microhardness is the average of at least 30 measurements on the transverse sections (HV_T). The minimum impression spacing (center to edge of the adjacent impression) was about 3 times the diagonal and was located at least 0.5 mm from the edge of the sample. To ensure cleanliness, the surfaces of the samples were polished prior to HV measurement. Each reading was an average of at least 10 separate measurements taken randomly on the surface of the samples. The highest and the lowest values of the 10 readings were disregarded. Some errors are inevitable during microhardness measurements. These errors are due to factors such as surface quality in homogeneities in the microstructure and ambiguity of indenter traces.

Equation [3] is also expressed as

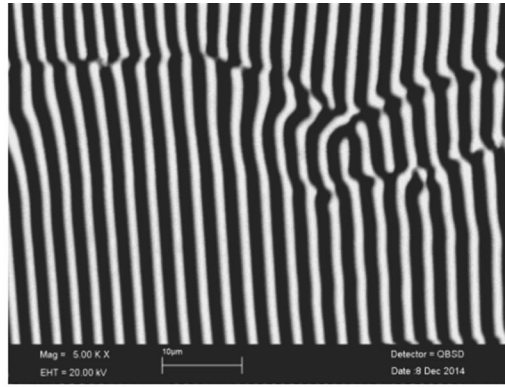
$$\text{HV} = 2 \frac{F}{A} \sin\left(\frac{\theta}{2}\right) \frac{1}{d^2} = 2 \frac{mg}{\pi r^2} \sin\left(\frac{\theta}{2}\right) \frac{1}{d^2}, \quad [4]$$

where m is the used load mass standardized (10 to 50 g), g is the gravitational acceleration (9.81 m s^{-2}), and r is the radius of sample (2 mm). The values of m , g , and θ are known. In the hardness measurements, the values of the sample radius (r) and diagonal length (d) are measured. Thus, the estimated experimental error in the measurement of HV is the sum of fractional uncertainty of the sample radius and diagonal length (d) and can be expressed as

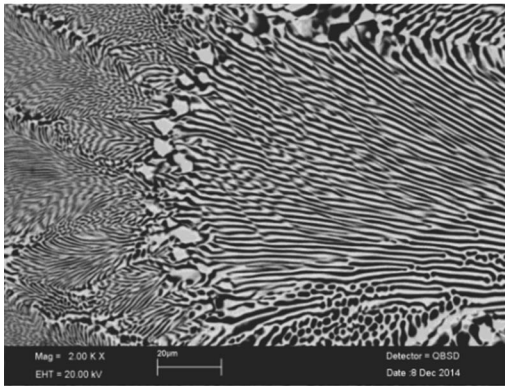
$$\left| \frac{\Delta \text{HV}}{\text{HV}} \right| = 2 \times \left| \frac{\Delta r}{r} \right| + 2 \times \left| \frac{\Delta d}{d} \right|. \quad [5]$$



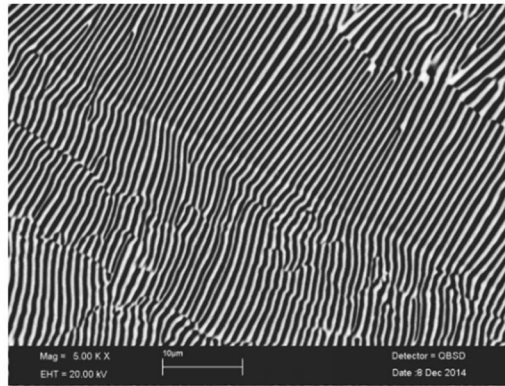
(a)



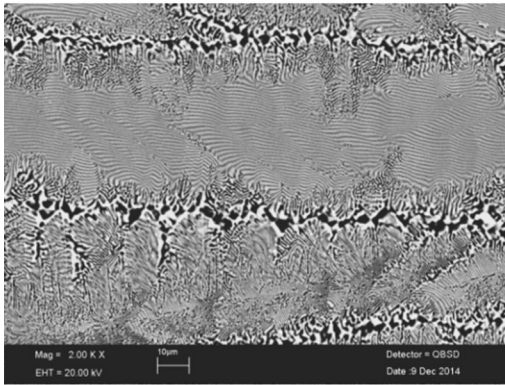
(b)



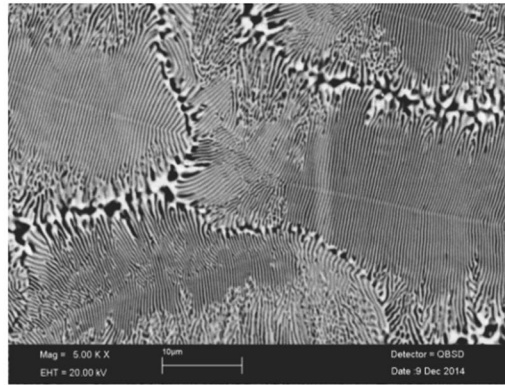
(c)



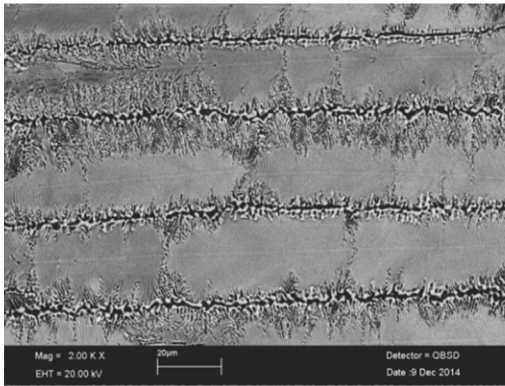
(d)



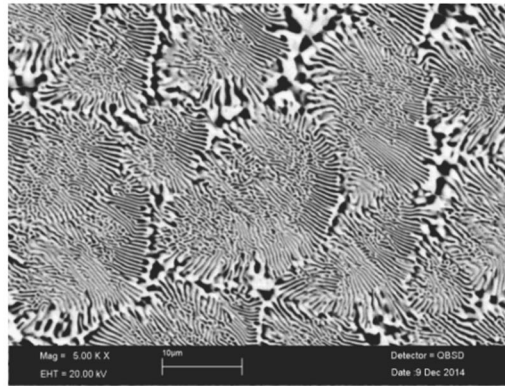
(e)



(f)



(g)



(h)

◀Fig. 1—Typical SEM images of the directionally solidified Al-32.5 wt pct Cu-1 wt pct Ni eutectic alloy at a constant temperature gradient of 4.93 K mm⁻¹: from (a) longitudinal and (b) transverse sections with $V = 9.25 \mu\text{m s}^{-1}$, from (c) longitudinal and (d) transverse sections with $V = 94.35 \mu\text{m s}^{-1}$, from (e) longitudinal and (f) transverse sections with $V = 1024.45 \mu\text{m s}^{-1}$, and from (g) longitudinal and (h) transverse sections with $V = 2056.68 \mu\text{m s}^{-1}$.

The values of r and d measured from the photographs are the sample and diagonal of the indentation trace. The fractional uncertainties for measurements of r and d are about 1 pct, respectively. Thus, the total estimated experimental error in the measurement of microhardness is about 4 pct.

D. Measurements of Ultimate Tensile Strength

One of the aims of the present work is to measure the tensile stress. The ultimate tensile strength (σ_{UTS}) values of the alloy were measured at room temperature with a Shimadzu Universal Testing Instrument (Type AG-10KNG) at a frequency of 10^{-3} s^{-1} . The data collected from the tensile test can be analyzed using the following formula to determine the stress (σ):

$$\sigma = \frac{F}{A} = \frac{mg}{\pi r^2}, \quad [6]$$

where σ is the stress in N mm^{-2} (or MPa), F is the applied force (N), and A is the original cross-sectional area of the sample. The uncertainty in the measurement of the UTS can be expressed in Eq. [6] as

$$\left| \frac{\Delta\sigma}{\sigma} \right| = 2 \times \left| \frac{\Delta r}{r} \right|. \quad [7]$$

Thus, the estimated experimental error in the measurement of the UTS is about 2 pct. Experimental error analyses of the measurements of λ , V , HV_T , and σ_{UTS} values were done and were reflected in all equations obtained by regression analysis.

The samples were prepared from directionally solidified rods with a diameter of 4 mm and length of 50 mm. The UTS measurements were repeated at least 3 times and the axis was taken parallel to the growth direction of the samples.

E. Determination of Elasticity

The metallic materials should have high strength and low elastic modulus. It can be seen in Figure 2 that the yield strength, elastic strain, and stress-strain curve in the elastic stage make up a triangle, and the mathematical expression of the elastic energy can be expressed as

$$\delta_e = \frac{1}{2} \sigma_e \sigma_y = \frac{\sigma_y^2}{2E}, \quad [8]$$

where δ_e is the elastic energy, σ_e is the elastic strain, σ_y is the yield strength, and E is the Young's modulus. According to Eq. [8], the elastic energy can be obtained from the stress-strain curve.

III. RESULTS AND DISCUSSION

A. Dependence of Eutectic Spacing on Low, High, and All Growth Rates

To determine individually the effect of LGR and HGRs (V) on eutectic spacing (microhardness (HV_T), and ultimate tensile strength (σ_{UTS}) at room temperature in the Al-Cu-Ni eutectic system, the samples were unidirectionally solidified with a wide range of growth rates (9.25 to $2056.68 \mu\text{m s}^{-1}$) at constant temperature gradient (4.93 K mm^{-1}) using a Bridgman-type growth apparatus.

The phase diagram of the Al-Cu-Ni system was determined by Zolotarevsky *et al.*^[40] According to the phase diagram of the Al-Cu-Ni system, the composition on the ternary eutectic point of the Al-Cu-Ni alloy is Al-32.5 wt pct Cu-1 wt pct Ni and the eutectic reaction in this point is $L \rightarrow \alpha\text{-Al}$ (matrix phase) solution + $\theta\text{-Al}_2\text{Cu}$ (intermetallic phase).^[40] Thus, the composition of the alloy was chosen to be Al-32.5 wt pct Cu-1 wt pct Ni to grow the two solid phases (Al solution and Al_2Cu) from the ternary liquid. SEM photographs of Al-32.5 wt pct Cu-1 wt pct Ni are given in Figure 1. The quantitative chemical composition analyses of α (Al solution) and θ (Al_2Cu intermetallic phase) were performed *via* energy-dispersive X-ray (EDX), as shown in Figure 3. According to EDX results, as shown in Figure 3(a), the gray phase is $\theta\text{-Al}_2\text{Cu}$ and the black phase is $\alpha\text{-Al}$ solution.

Table II. Values of Solidification Processing Parameters, Eutectic Spacing, Microhardness, Ultimate Tensile Strength, and Elastic Energy for Directionally Solidified Al-32.5 Wt Pct Cu-1 Wt Pct Ni Eutectic Alloy with Different Growth Rates at a Constant Temperature Gradient

Alloy (Wt Pct)	Solidification Parameters		Eutectic Spacing λ_T (μm)	Microhardness HV_T (kg mm^{-2})	Ultimate Tensile Strength σ_{UTS} (N mm^{-2})	Elastic Energy δ_e (MJ m^{-3})
	G (K mm^{-1})	V ($\mu\text{m s}^{-1}$)				
Al-32.5Cu-1Ni	4.93 ± 0.07	9.25 ± 0.19	3.09 ± 0.33	138.15 ± 5.41	181.96 ± 4.55	0.52
		46.40 ± 0.93	1.95 ± 0.21	149.21 ± 5.87	204.83 ± 4.88	0.61
		94.35 ± 1.89	1.08 ± 0.15	161.55 ± 6.38	217.43 ± 4.17	0.80
		162.85 ± 3.26	0.77 ± 0.10	172.74 ± 7.09	241.02 ± 5.23	1.12
		496.72 ± 9.93	0.59 ± 0.08	180.08 ± 6.99	252.15 ± 3.94	1.34
		1024.45 ± 20.49	0.51 ± 0.07	186.46 ± 7.48	265.86 ± 4.02	2.27
		1532.54 ± 30.65	0.44 ± 0.06	191.87 ± 7.33	273.47 ± 3.74	2.52
	2056.68 ± 41.13	0.38 ± 0.05	195.12 ± 7.62	278.21 ± 3.61	2.57	

Bold values in the table show measured experimental values for high growth rates.

λ_T : the average values of the eutectic spacings measured from the transverse section, HV_T : the average values of the microhardness measured from the transverse section, σ_{UTS} : the average values of the ultimate tensile strength measured from the longitudinal section.

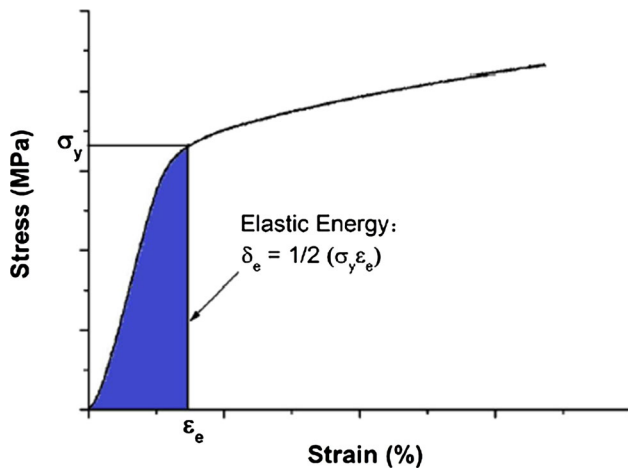


Fig. 2—Illustration of elastic energy in a stress–strain plot.

The eutectic spacing changes with the growth rates. At a constant temperature gradient (4.93 K mm^{-1}), the eutectic spacing decreases with the increasing growth rate and *vice versa*. The highest and lowest eutectic spacings were obtained with the growth rates of 9.25 and $2056.68 \mu\text{m s}^{-1}$, as shown in Figures 1(a) and (b) and Figures 1(g) and (h), respectively.

The measured values of λ_T variations with growth rates for Al-Cu-Ni alloy at constant G are given in Figure 4 and Table II. The changing of eutectic spacing with growth rate is linear on the logarithmic scale. The measured data create a straight line, as shown in Figure 4, and the proportionality equation can be obtained by the linear regression analysis as

$$\lambda = K_1 V^{-n}, \quad [9]$$

where K_1 is a constant and n is an exponent value of the growth rate.

The relationships between the eutectic spacing and growth rates were determined for directionally solidified Al-32.5 wt pct Cu-1 wt pct Ni alloy with LGRs, HGRs, and ALLGRs, respectively, at a constant G (4.93 K mm^{-1}) as

$$\lambda_{\text{LGR}} = (9.87 \pm 1.48)V^{-0.48} \text{ (for low growth rates)}, \quad [10a]$$

$$\lambda_{\text{HGR}} = (3.97 \pm 0.59)V^{-0.30} \text{ (for high growth rates)}, \quad [10b]$$

$$\lambda_{\text{ALLGR}} = (7.05 + 1.06)V^{-0.39} \text{ (for all growth rates)}. \quad [10c]$$

Experimental errors in the measurements of λ and V values are 13 and 2 pct, respectively, and they are included in Eq. [10].

There have been many attempts to classify the various types of microstructure that can be obtained by solidifying alloys near the eutectic composition. A useful approach for binary eutectic systems proposed by Jackson and Hunt^[21] relates the eutectic structure to the nature of growth of the individual phases of the eutectic. No accepted theoretical model for the exponent values of ternary eutectic systems exists. Thus, a comparison of experimental present results with previous similar experimental results^[41–44] and predicted values from the Jackson–Hunt eutectic theory^[21] for the Al-33 wt pct Cu eutectic alloy are given in Figure 4.

As shown in Figure 5, the lines of λ vs V for LGR and HGRs determined in the present work are between the lines of λ_T vs V determined by Çadırılı^[41] for Al-Cu, Kaygısız and Maraşlı^[42] for Al-Cu-Mg, Büyük *et al.*^[43] for Al-Cu-Ag, and Çadırılı *et al.*^[44] for Al-Cu-Co ternary eutectic alloys.

The lines of λ vs V for LGR and HGRs determined in the present work are slightly below the lines of λ_T vs V predicted from Jackson–Hunt eutectic theory^[21] and determined by Çadırılı^[41] for Al-Cu, Kaygısız and Maraşlı^[42] for Al-Cu-Mg, and Çadırılı *et al.*^[44] for Al-Cu-Co. However, the lines of λ vs V for LGR and HGRs determined in the present work are away from the line of λ_T vs V determined by Büyük *et al.*^[43] for Al-Cu-Ag. These high disparities are definitely due to the kind and amount of alloying elements of Ag, Cu, and Ni. The composition of the Al-Cu-Ag eutectic alloy was Al-17.6 wt pct Cu-42.2 wt pct Ag, and α (Al solution), β (Ag_2Al solution), and γ (Al_2Cu solution) phases were grown from the Al-Cu-Ag eutectic liquid.^[43] The composition of the Al-Cu-Ni eutectic alloy was Al-32.5 wt pct Cu-1 wt pct Ni, and α (Al solution) and γ (Al_2Cu solution) phases are grown from the Al-Cu-Ni eutectic alloy. Thus, the composition and microstructure of Al-Cu-Ag are different from the composition and microstructure of the Al-Cu-Ni eutectic alloy. These differences between them cause a microhardness difference between Al-Cu-Ni and Al-Cu-Ag eutectic alloys.

Furthermore, the exponent value of 0.48 relating to V for LGRs obtained in the present work is in good agreement within the little difference between the 0.46, 0.49, 0.45, and 0.50 values obtained by Wilde *et al.*^[19] for Al-25.6 wt pct Cu-24.5 wt pct Ag, Witusiewicz *et al.*^[28] for In-33.10 wt pct Bi-15.56 wt pct Sn, and Kaygısız and Maraşlı^[45] for Al-13.0 wt pct Si-5.0 wt pct Mg ternary alloys and predicted from the Jackson–Hunt eutectic theory,^[21] respectively. However, the exponent value of 0.30 relating to HGRs (V_{HGR}) determined in the present study is smaller than all exponent values relating to LGRs (V_{LGR}) given in Table III and predicted from the Jackson–Hunt eutectic theory.^[21] α and θ phases are grown from the eutectic liquid in Al-Cu-Ni, as assumed in the Jackson–Hunt eutectic theory.^[21] The exponent value of 0.30 relating to V , higher than $600 \mu\text{m s}^{-1}$ for the Al-Cu-Ni eutectic alloy obtained in the present work, is 60 pct smaller than the exponent value of 0.5 predicted by the Jackson–Hunt eutectic theory,^[21] while the exponent value of 0.48 relating to V , up to $600 \mu\text{m s}^{-1}$ for same alloy obtained in the present work, is very close to the exponent value of 0.5 predicted by the Jackson–Hunt

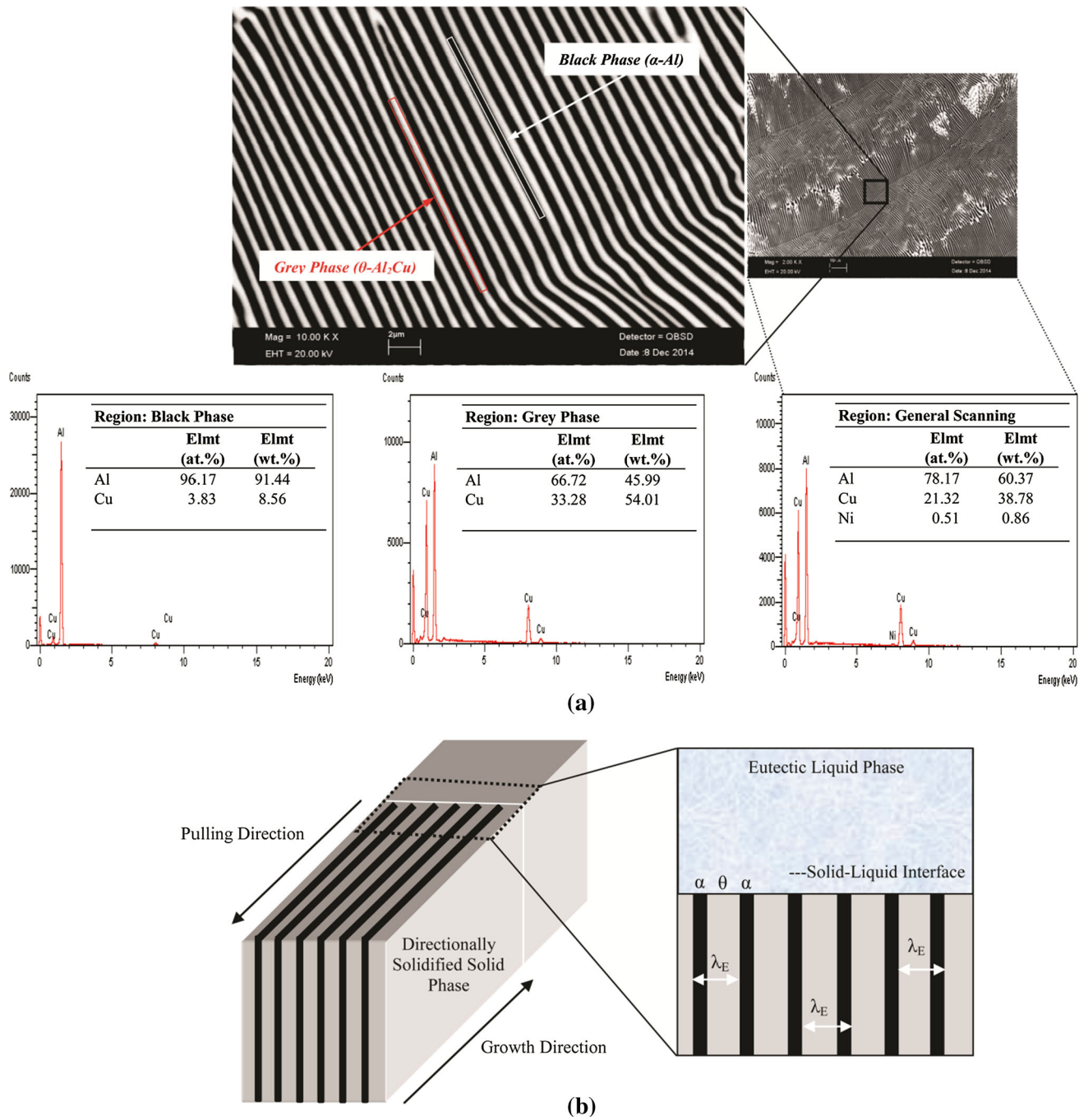


Fig. 3—(a) Chemical composition analysis of Al-32.5 wt pct Cu-1 wt pct Ni eutectic alloy by using SEM-EDX. The black phase is matrix α -Al phase, and the gray phase is θ -Al₂Cu intermetallic phase. (b) Solidification process of the eutectic structure and schematic illustration of measures of the microstructure.

eutectic theory.^[21] Thus, this difference might be due to HGRs (600 to 2100 $\mu\text{m s}^{-1}$) rather than the alloying elements of Cu and Ni.

Finally, as shown in Table III, the exponent value of 0.39 relating to all measurements of eutectic spacing for ALLGRs obtained in the present work is in good agreement with the exponent values obtained by only some of the different researchers^[42,46,47] for Al-based alloys.

The bulk growth rate value of 117.84 $\mu\text{m}^3 \text{s}^{-1}$ for LGRs obtained in the present work agrees with the bulk growth rates of 156, 139, 101.80, 112, and 101 $\mu\text{m}^3 \text{s}^{-1}$ obtained by Çadırılı *et al.*^[48] for Al-33.0 wt pct Cu, Tassa and Hunt^[49] for Al-35.5 wt pct Cu, Kaya *et al.*^[50] for Al-5.7 wt pct Ni, Jordan and Hunt^[51] for Al-32.0 wt pct Cu, and Wilde *et al.*^[19] for Al-25.6 wt pct Cu-24.5 wt pct Ag alloys, respectively. Even if the bulk growth rate

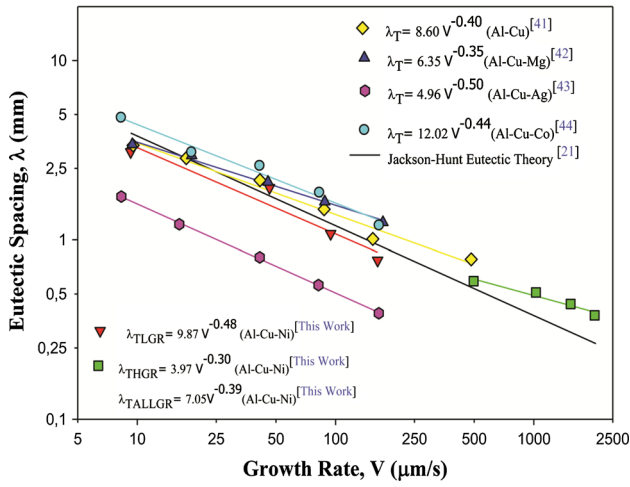


Fig. 4—Comparison of the eutectic spacing variation with the growth rate obtained in the present work with the eutectic spacing variation with the growth rate obtained in previous works^[41–44] for Al-based alloys and predicted from the Jackson–Hunt eutectic theory.^[21]

value of $258.27 \mu\text{m}^3 \text{s}^{-1}$ for HGRs obtained in the present work is quite larger than the aforementioned values, this value is very close to the values of 277.9, 232.17, 288, and 218.6 obtained by Mota *et al.*^[52] for Fe-22.8 at. pct Al-9.7 at. pct Nb alloys, Çadırlı *et al.*^[44] for Al-23.9 wt pct Cu-1.2 wt pct Co, Witusiewicz *et al.*^[28] for In-32.18 wt pct Bi-15.55 wt pct Sn, and Çadırlı *et al.*^[53] for In-33.10 wt pct Bi-15.56 wt pct Sn, respectively.

B. Effect of the Change in the Growth Rate (V) on Microhardness

The growth rate influences the microstructure and mechanical properties of metals. Directionally solidified materials have some advantages such as decreased microsegregation and refined microstructure.^[54,55] The mechanical properties of material change with its microstructure, and microstructure knowledge is necessary to produce advanced materials with desired properties.^[56–59]

According to Hall^[60] and Petch,^[61] the grain size depends on yield strength as

$$\sigma_y = \sigma_0 + \frac{K_2}{\sqrt{d}}, \quad [11]$$

where K_2 is a constant and d is the average grain size. The lamellar distance (depends on the average grain size. According to the eutectic theory, is proportional to the inverse square root of the growth rate (V). Thus, the Hall–Petch type relationships between microhardness and microstructure spacing or growth rate can be expressed as follows:

$$\text{HV} = \text{HV}_0 + K_3 \lambda^{-0.5}, \quad [12]$$

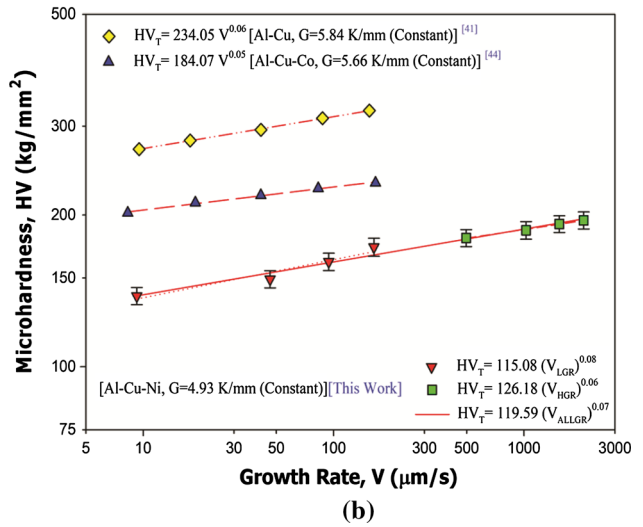
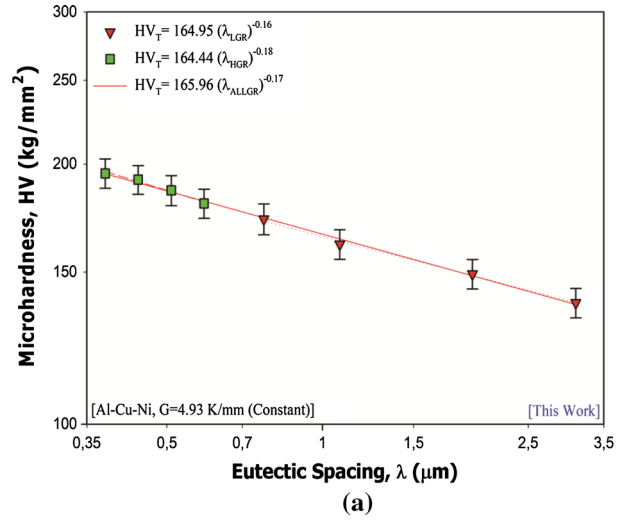


Fig. 5—Variation of microhardness (HV) as a function of (a) eutectic spacing and (b) growth rate for directionally solidified Al-Cu-Ni eutectic alloy obtained by linear regression analysis.

$$\text{HV} = \text{HV}_0 + K_4 V^{0.25}, \quad [13]$$

where HV_0 is the initial microhardness and K_3 and K_4 are the coefficients, which are related with the matters. In this work, the HV_0 , K_3 , and K_4 values were determined by fitting in Eqs. [5] and [6] the HV_T , and V measurement results obtained experimentally.

The aim of the present research is to determine the dependency of HV_T on V and for the Al-32.5 wt pct Cu-1 wt pct Ni directionally solidified alloy. The variations in the Hall–Petch type equations of microhardness (HV_T) as a function of eutectic spacing and HGRs (V) at a constant temperature gradient ($G = 4.93 \text{ K mm}^{-1}$) are plotted in Figures 5 and 6.

In the present work, the dependences of HV_T on eutectic spacing and LGR, HGR, and ALLGRs include the experimental errors in the measurements of HV_T , λ , and V values and were obtained as follows:

Table III. Comparison of the Values of Solidification Parameters, Microstructure, Microhardness and Ultimate Tensile Strength for Directionally Solidified Al-Cu-Ni Eutectic Alloy Obtained in the Present Work with the Values of Solidification Parameters, Microstructure, Microhardness, and Ultimate Tensile Strength for Al-Based Alloys Obtained in Previous Works

Alloy (Wt Pct)	G (K mm ⁻¹)	V (μm s ⁻¹)	Eutectic Spacing	Microhardness	Ultimate Tensile Strength
Al-32.5Cu-1Ni (This Work)	4.93	9.25 to 162.85	$\lambda_{TLGR} = 9.87V^{-0.48}$	$HV_T = 115.08V_{LGR}^{0.08}$	$\sigma_{UTS} = 146.55V_{LGR}^{0.09}$
		496.72 to 2056.68	$\lambda_{THGR} = 3.97V^{-0.30}$	$HV_T = 126.18V_{HGR}^{0.06}$	$\sigma_{UTS} = 163.68V_{HGR}^{0.07}$
		9.25 to 2056.68	$\lambda_{TALLGR} = 7.05V^{-0.39}$	$HV_T = 119.59V_{ALLGR}^{0.07}$	$\sigma_{UTS} = 153.11V_{ALLGR}^{0.08}$
Al-33Cu ^[41]	5.84	9.52 to 483.20	$\lambda_T = 8.60V^{-0.40}$	$HV_T = 234.05V^{0.06}$	$\sigma_{UTS} = 194.08V^{0.08}$
Al-30Cu-6Mg ^[42]	8.55	9.43 to 173.30	$\lambda_T = 6.35V^{-0.35}$	$HV_T = 308.30V^{0.03}$	$\sigma_{UTS} = 408.60V^{0.14}$
Al-17.6Cu-42.2Ag ^[43]	8.79	8.30 to 165.15	$\lambda_T = 4.96V^{-0.50}$	—	—
Al-17.6Cu-42.2Ag ^[62]	8.79	1.83 to 498.25	—	$HV_T = 181.97V^{0.10}$	—
Al-23.9Cu-1.2Co ^[44]	5.66	8.30 to 166.60	$\lambda_T = 12.02V^{-0.44}$	$HV_T = 184.07V^{0.05}$	—
Al-4.5Cu ^[46]	8.8	10 to 240	$\lambda_T = kV^{-0.38}$	—	—
Al-0.53Zn ^[46]			$\lambda_{Min} = 731.3V^{-0.38}$		
Al-0.26Mn ^[46]		10 to 200	$\lambda_{Max} = 8674.1V^{-0.53}$		
Al-2.4Cu ^[47]			$\lambda_T = kG^{-0.50}V^{-0.50}$	—	—
Al-4.4Cu ^[47]	5 to 13		$\lambda_T = kG^{-0.50}V^{-0.36}$		
Al-10.1Cu ^[47]		50 to 500	$\lambda_T = kG^{-0.50}V^{-0.43}$		
Al-(5.7-20)Cu ^[68]	2 to 9	7 to 430	$\lambda_T = 55G^{-0.50}V^{-0.25}$	—	—
Al-40Cu ^[69]	3.0	4.2 to 42	$\lambda_T = kV^{-0.32}$	—	—
Al-5.7Ni ^[51]	4.02	8.32 to 483.25	$\lambda_T = 10.76V^{-0.50}$	—	—
Al-5.7Ni ^[63]	4.02	8.32 to 483.25	—	$HV_T = 66.13V^{0.10}$	—
Al-6.5Ni-1.5Fe ^[64]			$\lambda_T = 10.80V^{-0.53}$	$HV_T = 42.54V^{0.07}$	$\sigma_{UTS} = 105.15V^{0.14}$
	4.48	8.25 to 164.80	$\lambda_T = 40.40V^{-0.48}$		
Al-11.1Si-4.2Ni ^[70]			$\lambda_T = 12.58V^{-0.50}$	—	—
	5.82	4.60 to 243.33	$\lambda_T = 7.94V^{-0.47}$		
Al-11.1Si-4.2Ni ^[65]	5.82	4.60 to 243.33	—	$HV_T = 72.44V^{0.08}$	$\sigma_{UTS} = 37.15V^{0.19}$
Al-13.0Si-5.0Mg ^[45]	9.39	8.64 to 165.20	$\lambda_T = 29.32V^{-0.45}$	$HV_T = 119.90V^{0.07}$	$\sigma_{UTS} = 222.84V^{0.20}$

$$HV_T = (105.5 \pm 4.2) + (1.86 \pm 0.32)\lambda_{LGR}^{-0.5}, \quad [14a]$$

$$HV_T = (119.8 \pm 4.8) + (1.49 \pm 0.25)\lambda_{HGR}^{-0.5}, \quad [14b]$$

$$HV_T = (109.1 \pm 4.4) + (1.72 \pm 0.29)\lambda_{ALLGR}^{-0.5}, \quad [14c]$$

$$HV_T = (103.3 \pm 4.1) + (106.1 \pm 6.37)V_{LGR}^{0.25}, \quad [15a]$$

$$HV_T = (144.2 \pm 5.8) + (42.54 \pm 2.55)V_{HGR}^{0.25}, \quad [15b]$$

$$HV_T = (124.4 \pm 5.0) + (62.16 \pm 3.73)V_{ALLGR}^{0.25}. \quad [15c]$$

As can be seen from Figures 5 and 6 and Eqs. [14] and [15], dependence of microhardness on both eutectic spacing and growth rate is stronger for LGRs than HGRs for directionally solidified Al-Cu-Ni eutectic alloy.

As can be seen from Figure 5(a), when the solidification parameters increase, the HV_T values increase. The relationship between HV_T and V was obtained by linear regression analysis and can be expressed as

$$HV_T = K_5 V^a, \quad [16]$$

where K_5 is a constant and a is the exponent value relating to the growth rate. Figure 5(b) shows the variation of HV_T as a function of V at a constant G and a comparison with the previous experimental result for similar alloy systems.^[41,44]

The relationships between HV_T - λ_T and HV_T - V , including the experimental errors in the measurements of HV_T , λ , and V values for LGR, HGR, and ALLGRs, were determined as

$$HV_T = (164.95 \pm 28.04)\lambda_{LGR}^{-0.16}, \quad [17a]$$

$$HV_T = (164.44 \pm 27.95)\lambda_{HGR}^{-0.18}, \quad [17b]$$

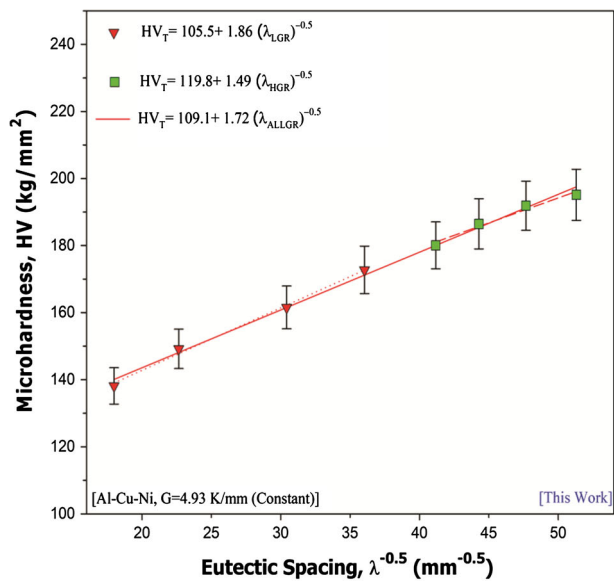
$$HV_T = (165.96 \pm 28.21)\lambda_{ALLGR}^{-0.17}, \quad [17c]$$

$$HV_T = (115.08 \pm 6.90)V_{LGR}^{0.08}, \quad [18a]$$

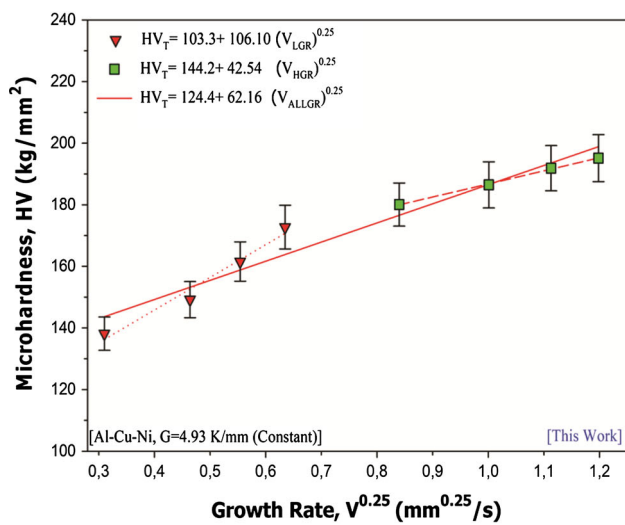
$$HV_T = (126.18 \pm 7.57)V_{HGR}^{0.06}, \quad [18b]$$

$$HV_T = (119.59 \pm 7.18)V_{ALLGR}^{0.07}. \quad [18c]$$

Experimental errors in the measurements of λ , HV_T , and V values are 13, 4, and 2 pct, respectively, and they are included in Eqs. [14], [15], [17], and [18].



(a)



(b)

Fig. 6—Variation of microhardness (HV) as a function of (a) eutectic spacing and (b) growth rate for directionally solidified Al-Cu-Ni eutectic alloy determined from the Hall-Petch type equations at a constant temperature gradient.

Çadırılı^[41] and Çadırılı *et al.*^[44] performed similar experimental work with a range of growth rates (9.52 to 483.20 and 8.30 to $\mu\text{m s}^{-1}$, respectively) at constant temperature gradients (5.84 and 5.66 K mm^{-1} , respectively) by using a Bridgman-type growth apparatus for Al-based alloys. As can be seen from Figures 5(b) and 6(b), the value of HV_T increases with the increase in the value of V and the decrease in the value of λ at a constant temperature gradient G . The dependences of HV_T on eutectic spacing and each range of growth rate for directionally solidified Al-32.5 wt pct Cu-1 wt pct Ni alloy are expressed with linear regression analysis. It can be seen from Figures 5(b) and 6(b) and Table II that the value of microhardness for Al-Cu-Ni eutectic alloy increases from 138.15 to $195.12 \text{ kg mm}^{-2}$ with an

increase in the growth rate from 9.25 to $2056.68 \mu\text{m s}^{-1}$. The exponent value of 0.07 for ALLGRs of the Al-Cu-Ni eutectic alloy is very close to the exponent values of 0.06 and 0.05 obtained for the Al-33.0 wt pct Cu^[41] and Al-23.9 wt pct Cu-1.2 wt pct Co eutectic alloys,^[44] respectively. However, the coefficient value of 119.59 for the Al-Cu-Ni eutectic alloy is nearly half the value of 234.05 and 184.07 obtained for the Al-Cu^[41] and Al-Cu-Co, respectively.^[44] This disagreement might be due to the HGRs and compositional dissimilarities obtained by adding alloying element Ni. The size of the α -Al and θ -Al₂Cu phases directs the properties and the alignment of colonies due to unidirectional solidification and is masked by the particle size effect.

Besides, as shown in Table III and the literature, the exponent value relating to ALLGRs (0.07) for directionally solidified Al-32.5 wt pct Cu-1 wt pct Ni alloy is in good agreement with the exponent values of 0.06 and 0.11 obtained by some researchers^[36,45,52,62–67] for ALLGRs.

C. Effect of Growth Rate on Ultimate Tensile Strength

As can be seen from Figures 7 and 8 and Table II, the value of ultimate tensile strength (σ_{UTS}) increases with the increase in the value of V and the decrease in the values of λ at a constant temperature gradient G . The relationships between the UTS and eutectic spacing and growth rates were obtained by using linear regression analysis. From Figure 7, the dependences of σ_{UTS} on eutectic spacing and LGR or HGRs for directionally solidified Al-32.5 wt pct Cu-1 wt pct Ni alloy were expressed with linear regression analysis.

Variations in UTS of Hall-Petch type equations with growth rate and eutectic spacing for the Al-Cu-Ni eutectic alloy are plotted in Figures 7(c) and (d). The dependences of σ_{UTS} on eutectic spacing and LGR, HGR, and ALLGRs, including the experimental errors in the measurements of HV_T , λ , and V values, were obtained as follows:

$$\sigma_{UTS} = 130.70 + 3.01\lambda_{LGR}^{-0.5}, \quad [19a]$$

$$\sigma_{UTS} = 151.40 + 2.52\lambda_{HGR}^{-0.5}, \quad [19b]$$

$$\sigma_{UTS} = 133.60 + 2.90\lambda_{ALLGR}^{-0.5}, \quad [19c]$$

$$\sigma_{UTS} = 125.70 + 174.40V_{LGR}^{0.25}, \quad [20a]$$

$$\sigma_{UTS} = 191.40 + 73.30V_{HGR}^{0.25}, \quad [20b]$$

$$\sigma_{UTS} = 158.80 + 105.40V_{ALLGR}^{0.25}. \quad [20c]$$

The relationships between σ_{UTS} - λ_T and σ_{UTS} - V , including the experimental errors in the measurements of HV_T , λ , and V values for LGR, HGR, and ALLGRs, were determined as

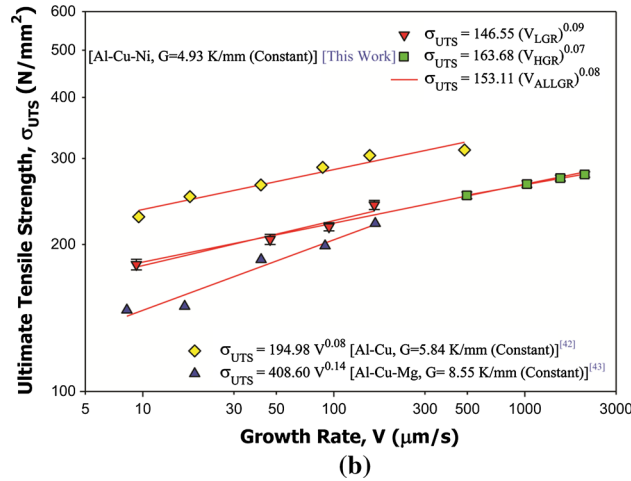
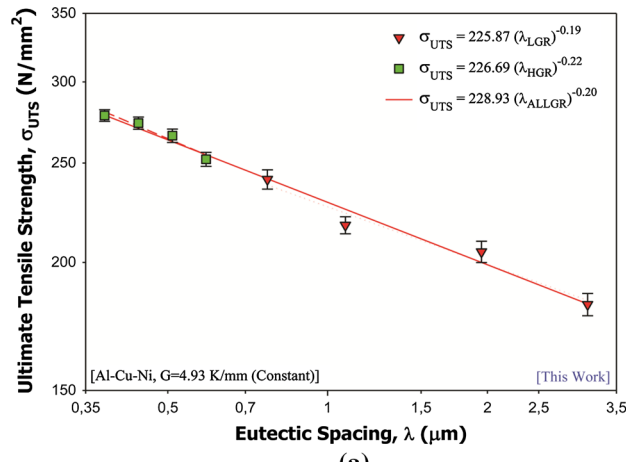


Fig. 7—Variations of ultimate tensile strength (σ_{UTS}) as a function of (a) eutectic spacing and (b) growth rates for directionally solidified Al-Cu-Ni eutectic alloy obtained by linear regression analysis at a constant temperature gradient.

$$\sigma_{UTS} = (225.87 \pm 33.88) \lambda_{LGR}^{-0.19}, \quad [21a]$$

$$\sigma_{UTS} = (226.69 \pm 34.00) \lambda_{HGR}^{-0.22}, \quad [21b]$$

$$\sigma_{UTS} = (228.93 \pm 34.34) \lambda_{ALLGR}^{-0.20}, \quad [21c]$$

$$\sigma_{UTS} = (146.55 \pm 5.86) V_{LGR}^{0.09}, \quad [22a]$$

$$\sigma_{UTS} = (163.68 \pm 6.55) V_{HGR}^{0.07}, \quad [22b]$$

$$\sigma_{UTS} = (153.11 \pm 6.12) V_{ALLGR}^{0.08}. \quad [22c]$$

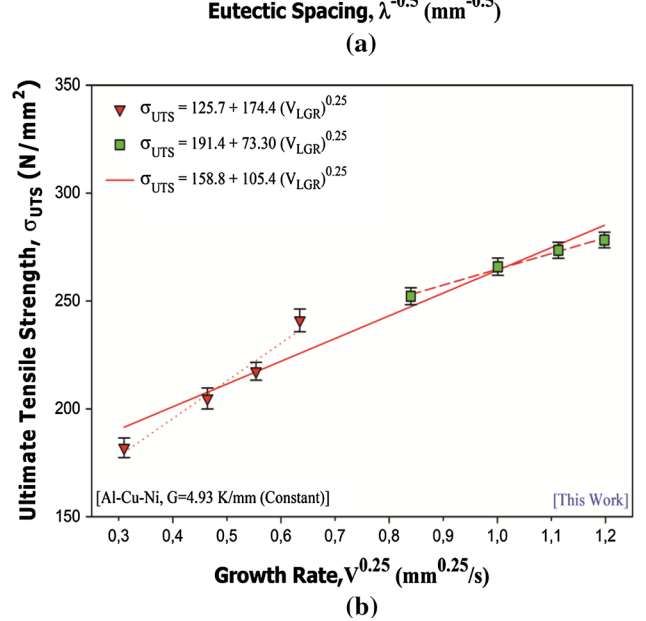
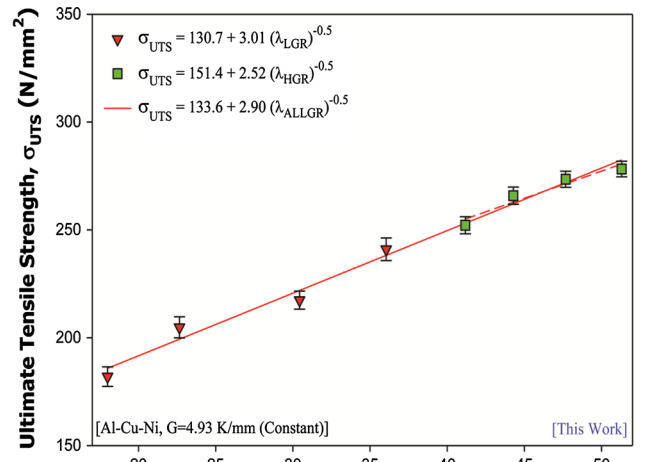


Fig. 8—Variations of ultimate tensile strength (σ_{UTS}) as a function of (a) eutectic spacing and (b) growth rates for directionally solidified Al-Cu-Ni eutectic alloy determined from Hall-Petch type equations at a constant temperature gradient.

Experimental errors in the measurements of λ , σ_{UTS} , and V values are 13, 2, and 2 pct, respectively, and they are included into Eqs. [14], [15], [17], and [18].

Variations of UTS with eutectic spacing and growth rate for the Al-Cu-Ni eutectic alloy are plotted in Figures 7 and 8. It can be seen from Figures 7 and 8 and Table II that the value of UTS for the Al-Cu-Ni eutectic alloy increases from 181.96 to 278.21 N mm⁻² with increasing growth rate from 9.25 to 2056.68 μm s⁻¹. A comparison of the present results with the experimental results obtained in previous works for Al-Cu^[41] and Al-Cu-Mg^[42] alloys is also given in Figures 7 and 8. The exponent value of 0.08 obtained for ALLGRs of the Al-Cu-Ni eutectic alloy is in good agreement with the

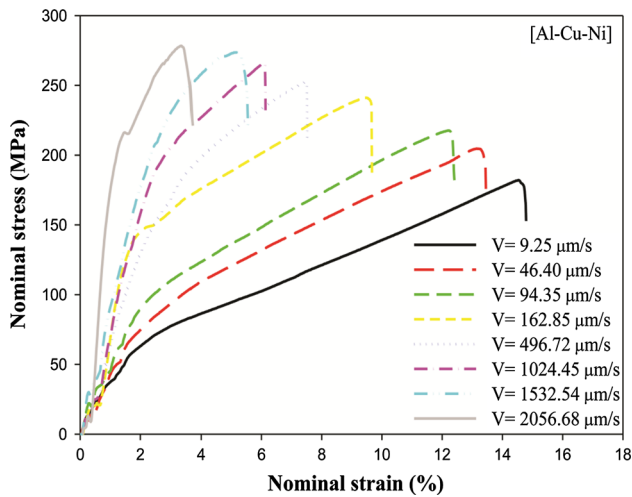


Fig. 9—Nominal stress–strain curves for the Al-Cu-Ni eutectic alloy directionally solidified with different growth rates (9.25 to 2056.68 $\mu\text{m s}^{-1}$) at a constant temperature gradient of 4.93 K mm^{-1} .

exponent value of 0.08 obtained for Al-33.0 wt pct Cu.^[41] However, the exponent value of 0.08 obtained for Al-32.5 wt pct Cu-1 wt pct Ni is nearly half of the exponent value of 0.14 obtained for Al-30 wt pct Cu-6 wt pct Mg.^[41] Likewise, the coefficient value of 153.11 obtained for Al-Cu-Ni eutectic alloy is close to the coefficient value of 194.08 obtained in Reference 41 but is one-third the coefficient value of 480.60 obtained in Reference 42. After this comparison, it can be concluded that the UTS values are affected by the alloying elements of Cu, Mg, and Ni and growth rates.

D. Effect of Growth Rate on Elastic Energy

The stress–strain curves for directionally solidified Al-Cu-Ni alloy with different growth rates are plotted in Figure 9.

The elastic energies for directionally solidified Al-Cu-Ni alloy with different growth rates were obtained from the stress–strain curves and are given in Table II. According to the stress–strain curves for directionally solidified Al-Cu-Ni alloy with different growth rates, the value of strain energy increases from 0.52 MPa (MJ m^{-3}) to 2.57 MPa as the growth rate increases from 9.25 m s^{-1} to 2056.68 $\mu\text{m s}^{-1}$. The strain energy of materials can be calculated from the dislocation density. It was found that the maximum strain energy stored as dislocations was calculated to be about 0.226 MJ m^{-3} in pure Cu and about 0.040 MJ m^{-3} in pure Al.^[71]

The minimum value of 0.52 MPa calculated in the present work for the directionally solidified Al-Cu-Ni alloy with LGR is in a good agreement with the calculated value of 0.226 MPa for pure Cu.^[71] However, the maximum value of 2.57 MPa calculated in the present work for the directionally solidified Al-Cu-Ni alloy at HGR is 10 times larger than the calculated value of 0.0226 MPa for pure Copper.^[71] This difference

implies that the stored energy is dependent on the growth rates for the directionally solidified Al-32.5 wt pct Cu-1 wt pct Ni eutectic alloy.

IV. CONCLUSIONS

In the present work, Al-32.5 wt pct Cu-1 wt pct Ni (Al-based) eutectic alloy was directionally solidified with a wide range of growth rates at a constant temperature gradient and then the microstructure, microhardness, and UTS were investigated. The principal results obtained in this work are as follows.

- (1) The exponent value of 0.30 related to the growth rate for directionally solidified Al-32.5 wt pct Cu-1 wt pct Ni alloy with a wide range of growth rates differs from the exponent value predicted with the Jackson–Hunt eutectic theory^[21] and obtained in previous experimental works. The exponent value related to the growth rate up to the growth rate of 600 $\mu\text{m s}^{-1}$ for Al-32.5 wt pct Cu-1 wt pct Ni alloy is in good agreement with the predicted exponent value of 50 related to growth by the Jackson–Hunt eutectic theory^[21] but differs from the predicted value of 0.50 by the Jackson–Hunt eutectic theory^[21] at the HGR of above than 600 $\mu\text{m s}^{-1}$.
- (2) The variations in the Hall–Petch type equations and dependences of microhardness and UTS on growth rate were obtained for LGR, HGR, and ALLGRs at a constant ($G = 4.93 \text{ K mm}^{-1}$). The results obtained in the present work were compared with similar experimental results in the literature.
- (3) From the plots of the stress–strain, the elastic energies for directionally solidified Al-Cu-Ni alloy with different growth rates were obtained. It was observed that the elastic energy for directionally solidified Al-32.5 wt pct Cu-1 wt pct Ni eutectic alloy depends on growth rates.

ACKNOWLEDGMENTS

This work was supported by the Erciyes University Scientific Research Project Unit under Contract No. FDK-2013-4741. The researchers are thankful for this financial support.

REFERENCES

1. D.A. Porter and K.E. Easterling: *Phase Transformations in Metals and Alloys*, 2nd ed., CRC Press, Boca Raton, FL, 1992.
2. R. Caram and S. Milenkovic: *J. Cryst. Growth*, 1999, vol. 198, pp. 844–49.
3. H.Z. Fu and L. Liu: *Mater. Sci. Forum*, 2005, vols. 475–479, pp. 607–12.
4. H. Jones: *Rapid Solidification of Metals and Alloys*, The Institution of Metallurgists, Sheffield, 1982.
5. J.G. Kaufman and E.L. Rooy: *Aluminum Alloy Castings: Properties, Processes, and Applications*, ASM International, Materials Park, OH, 2004.

6. Y.S. Sun, G.W. Lorimer, and N. Ridley: *Metall. Trans. A*, 1990, vol. 21A, pp. 575–88.
7. C.C. Jia, K. Ishida, and T. Nishizawa: *Metall. Mater. Trans. A*, 1994, vol. 25A, pp. 473–85.
8. V. Pelosin and A. Riviere: *J. Alloys Compd*, 1998, vol. 268, pp. 166–72.
9. X.J. Liu, C.P. Wang, I. Ohnuma, R. Kainuma, and K. Ishida: *J. Phase Equilib.*, 2001, vol. 22, pp. 431–38.
10. C.H. Wang, S.W. Chen, C.H. Chang, and J.C. Wu: *Metall. Mater. Trans. A*, 2003, vol. 34A, pp. 199–209.
11. Materials Science International Team: *Light Metal Systems, Part 2 Volume 11A2, of the Series Landolt–Börnstein–Group IV Physical Chemistry Al–Cu–Ni (Aluminium–Copper–Nickel)*, 2005, pp. 1–23.
12. M. Rhême, F. Gonzales, and M. Rappaz: *Scripta Mater.*, 2008, vol. 59, pp. 440–43.
13. F. Gonzales and M. Rappaz: *Metall. Mater. Trans. A*, 2006, vol. 37A, pp. 2797–806.
14. A.E. Ares, S.F. Gueijmanb, R. Caramc, and C.E. Schvezov: *J. Cryst. Growth*, 2005, vol. 275, pp. 319–27.
15. C. Yang, B.S. Li, M.X. Ren, and H.Z. Fu: *Int. J. Adv. Manuf. Technol.*, 2010, vol. 46, pp. 173–78.
16. A.E. Ares, L.M. Gassac, S.F. Gueijmanb, and C.E. Schvezova: *J. Cryst. Growth*, 2008, vol. 420, pp. 1355–61.
17. W.R. Osório, C.M.A. Freire, and A. Garcia: *J. Mater. Sci.*, 2005, vol. 40, pp. 4493–99.
18. W.R. Osório, J.R. Spinelli, N. Cheung, and A. Garcia: *Mater. Sci. Eng. A*, 2006, vol. 420, pp. 179–86.
19. J. De Wilde, L. Froyen, and S. Rex: *Scripta Mater.*, 2004, vol. 51, pp. 533–38.
20. C. Zhang, Y. Wu, M. Fang, S. Wu, X. We, Y. Cheng, and Y. Sun: *Chin. Sci. Bull.*, 1997, vol. 42 (24), pp. 2067–72.
21. K.A. Jackson and J.D. Hunt: *Trans. TMS-AIME*, 1966, vol. 236, pp. 1129–42.
22. V. Datye and J.S. Langer: *Phys. Rev. B*, 1981, vol. 24, pp. 4155–69.
23. V. Seetharaman and R. Trivedi: *Metall. Trans. A*, 1988, vol. 19A, pp. 2955–64.
24. R. Trivedi, J.T. Mason, J.D. Verhoeven, and W. Kurz: *Metall. Trans. A*, 1991, vol. 22A, pp. 2523–33.
25. A. Ourdjini, J. Liu, and R. Elliott: *Mater. Sci. Technol. Lond.*, 1994, vol. 10, pp. 312–18.
26. H. Kaya, E. Çadırılı, and M. Gündüz: *J. Mater. Process. Technol.*, 2007, vol. 183, pp. 310–20.
27. H. Kaya, E. Çadırılı, and M. Gündüz: *J. Mater. Eng. Perform.*, 2003, vol. 12, pp. 456–69.
28. V.T. Witusiewicz, U. Hecht, S. Rex, and M. Apel: *Acta Mater.*, 2005, vol. 53, pp. 3663–69.
29. E. Çadırılı, H. Kaya, and N. Maraşlı: *Metall. Mater. Int.*, 2009, vol. 15, pp. 741–51.
30. M. Gündüz, H. Kaya, E. Çadırılı, and A. Özmen: *Mater. Sci. Eng. A*, 2004, vol. 369, pp. 215–29.
31. E. Çadırılı, H. Kaya, and M. Gündüz: *Mater. Res. Bull.*, 2003, vol. 38, pp. 1457–76.
32. E. Çadırılı, H. Kaya, and M. Gündüz: *J. Alloys Compd*, 2007, vol. 431, pp. 171–79.
33. R. Trivedi, P. Magnin, and W. Kurz: *Acta Metall.*, 1987, vol. 35, pp. 971–80.
34. J.N. Clark and R. Elliott: *J. Cryst. Growth*, 1976, vol. 33, pp. 169–73.
35. S.M.D. Borland and R. Elliott: *Metall. Trans. A*, 1987, vol. 9A, pp. 1063–67.
36. S. Khan, A. Ourdjini, Q.S. Hamed, M.A.A. Najafabadi, and R. Elliott: *J. Mater. Sci.*, 1993, vol. 28, pp. 5957–62.
37. E. Çadırılı and M. Gündüz: *J. Mater. Process. Technol.*, 2000, vol. 97, pp. 74–81.
38. M. Asta, C. Beckermann, A. Karma, W. Kurz, R. Napolitano, M. Plapp, G. Purdy, M. Rappaz, and R. Trivedi: *Acta Mater.*, 2009, vol. 57, pp. 941–71.
39. E. Acer, H. Erol, and M. Gündüz: *Light Metals Technology Book Series Materials Science Forum*, 2013, vol. 765, pp. 215–19.
40. V.S. Zolotarevsky, N.A. Belov, and M.V. Glazoff: *Casting Aluminum Alloys*, Elsevier, Pittsburgh, PA, 2007, pp. 34–35.
41. E. Çadırılı: *Met. Mater. Int.*, 2013, vol. 19, pp. 411–22.
42. Y. Kaygısız and N. Maraşlı: *Phys. Met. Metallogr.*, 2017, vol. 118, pp. 389–98.
43. U. Böyük, N. Maraşlı, H. Kaya, E. Çadırılı, and K. Keşlioğlu: *Appl. Phys. A*, 2009, vol. 95, pp. 923–32.
44. E. Çadırılı, I. Yilmazer, M. Sahin, and H. Kaya: *Trans. Indian Inst. Met.*, 2015, vol. 68, pp. 817–27.
45. Y. Kaygısız and N. Maraşlı: *J. Alloys Compd*, 2015, vol. 618, pp. 197–203.
46. X. Lin, W.D. Huang, J. Feng, T. Li, and Y. Zhou: *Acta Metall.*, 1999, vol. 47, pp. 3271–80.
47. K.P. Young and D.H. Kirkwood: *Metall. Trans. A*, 1975, vol. 6A, pp. 197–205.
48. E. Çadırılı, A. Ülgen, and M. Gündüz: *Mater. Trans. JIM*, 1999, vol. 40, pp. 989–96.
49. M. Tassa and J.D. Hunt: *J. Cryst. Growth*, 1976, vol. 34, pp. 38–48.
50. H. Kaya, U. Böyük, E. Çadırılı, and M. Gündüz: *Kov. Mater.*, 2010, vol. 48, pp. 291–300.
51. R.M. Jordan and J.D. Hunt: *Mater. Trans.*, 1971, vol. 2, pp. 3401–10.
52. M.A. Mota, A.A. Coelho, J.M.Z. Bejarano, S. Gama, and R. Caram: *J. Alloys Compd*, 2005, vol. 399, pp. 196–201.
53. E. Çadırılı, U. Böyük, H. Kaya, N. Maraşlı, K. Keşlioğlu, S. Akbulut, and Y. Ocak: *J. Alloys Compd*, 2009, vol. 470, pp. 150–56.
54. A. Munitz: *Metall. Trans. B*, 1985, vol. 16B, pp. 149–61.
55. M. Zimmermann, M. Carrard, and W. Kurz: *Acta Metall.*, 1989, vol. 37, pp. 3305–13.
56. N. Cheung, M.C.F. Ierardi, A. Garcia, and R. Vilar: *Lasers*, 2000, vol. 10, pp. 275–91 (in English).
57. W.R. Osório and A. Garcia: *Mater. Sci. Eng. A*, 2002, vol. 325 (1–2), pp. 103–11.
58. J. Quaresma, C.A. Santos, and A. Garcia: *Metall. Mater. Trans. A*, 2000, vol. 31A (12), pp. 3167–78.
59. C. Siqueira, N. Cheung, and A. Garcia: *Metall. Mater. Trans. A*, 2002, vol. 33A, pp. 2107–18.
60. E.O. Hall: *Proc. Phys. Soc. B*, 1951, vol. 64 (9), pp. 747–53.
61. N.J. Petch: *J. Iron Steel Inst.*, 1953, vol. 174, pp. 25–28.
62. U. Böyük, N. Maraşlı, H. Kaya, E. Çadırılı, and K. Keşlioğlu: *Curr. Appl. Phys.*, 2012, vol. 12, pp. 7–10.
63. H. Kaya, U. Böyük, E. Çadırılı, and N. Maraşlı: *Mater. Des.*, 2012, vol. 34, pp. 707–12.
64. S. Engin, U. Böyük, and N. Maraşlı: *J. Alloy Compd*, 2016, vol. 660, pp. 23–31.
65. U. Böyük: *Met. Mater. Int.*, 2012, vol. 18, pp. 933–38.
66. J. Fan, X. Li, Y. Su, J. Guo, and H. Fu: *Mater. Des.*, 2012, vol. 34, pp. 552–58.
67. J. Fan, X. Li, Y. Su, J. Guo, and H. Fu: *J. Alloy Compd*, 2010, vol. 504 (1), pp. 60–64.
68. M.A. Taha: *Met. Sci.*, 1979, vol. 13, pp. 9–12.
69. M.D. Dupouy, D. Camel, and J.J. Favier: *Acta Metall.*, 1992, vol. 40, p. 1791.
70. U. Böyük, S. Engin, and N. Maraşlı: *Mater. Charact.*, 2011, vol. 62, pp. 844–51.
71. Y. Murata, I. Nakaya, and M. Morinaga: *Metall. Mater. Trans. B*, 2008, vol. 49B, pp. 20–23.